Title	Ionic liquid electrolytes with high sodium ion fraction for high-rate and long-life sodium secondary batteries
Author(s)	Chen, Chih Yao; Kiko, Tomohiro; Hosokawa, Takafumi; Matsumoto, Kazuhiko; Nohira, Toshiyuki; Hagiwara, Rika
Citation	Journal of Power Sources (2016), 332: 51-59
Issue Date	2016-11-15
URL	http://hdl.handle.net/2433/224788
Right	© 2016. This manuscript version is made available under the CC-BY-NC-ND 4.0 license http://creativecommons.org/licenses/by-nc-nd/4.0/; The full-text file will be made open to the public on 15 November 2018 in accordance with publisher's 'Terms and Conditions for Self-Archiving'; This is not the published version. Please cite only the published version. この論文は出版社版でありません。引用の際には出版社版をご確認ご利用ください。
Type	Journal Article
Textversion	author

Ionic liquid electrolytes with high sodium ion fraction for high-rate and long-life sodium secondary batteries

Chih-Yao Chen[a], Tomohiro Kiko[a], Takafumi Hosokawa[a],

Kazuhiko Matsumoto[a,*], Toshiyuki Nohira[b,*], Rika Hagiwara[a]

[a]Graduate School of Energy Science, Kyoto University, Sakyo-ku, Kyoto 606-8501, Japan

[b]Institute of Advanced Energy, Kyoto University, Gokasho, Uji, Kyoto 611-0011, Japan

*Corresponding authors: Kazuhiko Matsumoto, Toshiyuki Nohira

E-mail addresses:

k-matsumoto@energy.kyoto-u.ac.jp

nohira.toshiyuki.8r@kyoto-u.ac.jp

Tel: +81-75-753-5822

Fax: +81-75-753-5906

Abstract

Sodium secondary batteries are attracting considerably renewed interest as new battery systems owing to the high and uniform abundance and cost advantages of Na. However, their performance is still far from optimal as compared to the well-developed Li-ion technology. Herein, Na secondary batteries with unprecedented rate capability and a long life has been achieved by using a highly concentrated bis(fluorosulfonyl)amide anion (FSA^-)-based ionic liquid electrolyte (3.3 mol dm^{-3} Na[FSA]) and a $Na_2FeP_2O_7$ positive electrode, in a targeted operating temperature range from room to intermediate. Nearly full discharge capacity is obtained at 4000 mA g^{-1}, and 79% of the capacity is retained at a discharge rate as high as 20000 mA g^{-1} at 363 K. Stable cycling (>300 cycles) with satisfactory coulombic efficiency (>99.5%) is found at an intermediate rate (100 mA g^{-1}) over 298–363 K. A high-rate cycling test (1000 mA g^{-1}) at 363 K reveals that the cell could retain 93 % of its initial capacity after 1500 cycles.

Key words: sodium secondary batteries, ionic liquids, pyrophosphates, bis(fluorosulfonyl)amide

1. Introduction

Driven by the exponentially growing demand for large-scale stationary and vehicular energy storage devices, Na secondary batteries have received renewed research interest owing to the high and uniform abundance, cost advantages, and environmental benignity of Na [1–4]. Sodium and lithium secondary batteries share many similarities: for example, the Na^+-conducting electrolytes that have been investigated are mainly based on nonaqueous organic solvents (typically, propylene carbonate), which parallel the well-developed Li-ion technology [4–6]. However, the diverse applications expected for Na secondary batteries pose requirements different from those for portable electronics, including a high level of safety, long cycle life, and wide working-temperature span, as well as fast charging/discharging capabilities. The further development of possible electrolyte materials is therefore essential [7].

Ionic liquids (ILs) are potentially ideal candidates for this pursuit, owing to their unique suite of properties, including low flammability, negligible vapor pressure, wide liquidus temperature, and high electrochemical/thermal stability [8,9]. Despite these advantages, only a few publications have detailed IL electrolytes for use in Na secondary batteries [10–13], for several reasons. First, a larger interfacial impedance is generally observed for Na cells than for the Li equivalents [14,15], primarily caused by the unstable solid electrolyte interphase (SEI) film that forms on Na metal [4].

Second, ILs typically exhibit high viscosity and inferior ionic conductivity compared to conventional organic electrolytes [5]. Consequently, Na batteries applying ILs have been tested at very low rates (e.g., 10–20 mA g^{-1}) and show a strong trade-off between accessible capacity and charge/discharge rates in most cases [11–13]. In our previous studies, the physical properties of a series of purely inorganic [16] and inorganic-organic hybrid [17–20] IL electrolytes based on the bis(fluorosulfonyl)amide anion (FSA^-) were evaluated for Na secondary battery applications. Electrochemical performance as a function of temperature (between 253 and 363 K) was tested for a range of positive and negative electrode materials utilizing Na[FSA]–[C_3C_1pyrr][FSA] (C_3C_1pyrr: *N*-propyl-*N*-methylpyrrolidinium) in both half and full cells [21–25]. The results indicate that elevation of the operating temperature effectively facilitates ion transport in the electrolyte and electrode, permitting the cells to be cycled at a current density of 2360 mA g^{-1} and discharged at a current density higher than 4000 mA g^{-1} when combined with a suitable electrode material [22–24]. Although temperatures above 323 K may be considered too high for battery operation, they are practicable and even preferable with the aid of thermally and chemically stable ionic liquid electrolytes. Such environments are not particularly rare, if one considers the engine compartments of automobiles or the constant waste heat generated from devices or machines that operate in our daily lives or industrially.

Alternatively, if the environment is not at an elevated temperature, batteries working at high rates are easily self-heated under appropriate insulating conditions.

Recently, superconcentrated electrolytes composed of aprotic solvents with high Li salt concentrations (i.e., > 3 mol dm^{-3}) have received intense attention in the Li battery research community [26–33]. This new class of electrolytes offers unusual functionality including the facilitated formation of passivation films [26], inhibited dendritic Li deposition [27,28], suppressed corrosion of Al current collectors [29], and enhanced reductive or oxidative stability [30,31]. Most importantly, ultrafast electrode kinetics was found for particular systems utilizing Li[FSA], in spite of their high viscosities [28,30,32]. These phenomena were attributed to entirely different solution structures between the highly concentrated electrolyte and the corresponding dilute electrolyte [33]. Our prior work using Na[FSA]–[C_3C_1pyrr][FSA] showed that the rate capability of the $NaCrO_2$ positive electrode could be improved by adjusting the Na[FSA] content [18]. Layered-structured sodium transition metal oxides (such as $NaCrO_2$) are attractive intercalation hosts; however, they are prone to undergo successive phase transformations induced by oxygen layer glides at specific Na contents [2–4]. The kinetic energy barrier for the phase transition is a complex interplay of multiple experimental factors, making a comprehensive understanding of the electrochemical results challenging.

To clarify the role of the electrolyte in improved electrode kinetics, an electrode material that has been thoroughly studied is preferable. Further, it must be a good Na host material, allowing the reversible and facile insertion and extraction of Na^+. The $Na_2FeP_2O_7$ positive electrode was first reported by Yamada et al. in 2012 [34]. Atomistic simulation studies revealed that $Na_2FeP_2O_7$ supports favorable three-dimensional Na ion diffusion paths with acceptably low activation energies, and hence, high Na^+ mobility [35]. This assertion was experimentally verified in a number of publications [36–38], including ours involving ILs [24,39]. In this work, the electrode characteristics of $Na_2FeP_2O_7$ positive electrodes in the Na[FSA]–[C_2C_1im][FSA] (C_2C_1im: 1-ethyl-3-methylimidazolium) IL electrolytes were investigated as a function of both Na salt fraction and working temperature. This imidazolium-based IL exhibits higher ionic conductivity and lower viscosity than the corresponding pyrrolidinium-based IL [19,20]. Transport and structural properties are described in the first part of the paper. The electrochemical behavior discussed in the following part focuses on the differences between the Na[FSA]–[C_2C_1im][FSA] and Na[FSA]–[C_3C_1pyrr][FSA] systems, as well as the rate capability and cyclability.

2. Experimental

2.1 Materials

The FSA salts, Na[FSA] (Mitsubishi Materials Electronic Chemicals, water content < 72 ppm), [C_2C_1im][FSA] (Kanto Chemical, water content < 28 ppm), and [C_3C_1pyrr][FSA] (Kanto Chemical, water content < 30 ppm) were dried under vacuum at 363 K for 24 h prior to use. To compare the effects of the imidazolium- and pyrrolidinium-based ILs, Na[FSA]–[C_2C_1im][FSA] and Na[FSA]–[C_3C_1pyrr][FSA] were prepared at the same Na[FSA] fraction of 30 mol%. To investigate the effects of Na salt content on the physical and electrochemical properties, Na[FSA]–[C_2C_1im][FSA] ILs at Na[FSA] fractions of 0, 10, 20, 30, 40, and 50 mol% were also prepared. The apparent transport number was measured for a symmetric Na/Na 2032 type coin cell at 363 K using an ac-dc method [40,41], as described in our previous study (see Ref. 19 for a discussion of the apparent transport number concept). Measurements at each concentration were performed at least three times to ensure reproducibility. Raman spectra were recorded at 298 and 363 K using a Nanofinder 30 (Tokyo Instruments Inc.) microfocus Raman spectrometer with a 532 nm He-Ne laser. Peak deconvolution of the Raman spectra was performed using the Voigt function. Table 1 lists the IL electrolytes used in this work with their ionic conductivities (σ(IL)), apparent transport numbers of Na^+ ($t'(Na^+)$), and Na^+ ion conductivities ($\sigma(Na^+)$). Sodium iron pyrophosphate, $Na_2FeP_2O_7$, was synthesized by a conventional solid-state method, as reported previously [39]. The starting materials

Table 1. Selected physicochemical properties of the Na[FSA]−[C_2C_1im][FSA] IL electrolytes

Na[FSA] fraction (mol%)	molar conc. (mol dm^{-3})	molar ratio (FSA:Na)	σ (IL) (ms cm^{-1})[a)]	t' (Na^+)[b)]	σ (Na^+) (ms cm^{-1})[c)]
0	-	-	54.4	-	-
10	0.503	10	45.7	0.13	5.94
20	1.069	5.0	38.3	0.19	7.28
30	1.704	3.3	31.1	0.25	7.78
40	2.428	2.5	23.8	0.27	6.43
50	3.263	2.0	16.9	0.35	5.92

[a)]Ionic conductivity measured at 363 K [20]

[b)]Apparent transport number of Na^+ measured at 363 K

[c)]Na^+ ion conductivity, calculated by multiplying σ (IL) and t' (Na^+)

Na_2CO_3, $FeC_2O_4{\cdot}2H_2O$, and $(NH_4)_2HPO_4$ were stoichiometrically mixed by wet planetary ball-milling (Fritsch Pulverisette 7 Premium Line) in acetone at 600 rpm for 8 h. After evaporating the acetone, the mixture was ground and then initially heated at 573 K for 6 h. The calcined sample was reground and heated again at 873 K for 12 h. The heat treatment was carried out under a steady flow of either Ar or Ar/H_2 (95:5). Pulverization of the obtained sample was conducted using an agate mortar in either an Ar-filled glovebox or ambient air. Crystal structures of the prepared $Na_2FeP_2O_7$ samples were analyzed by X-ray diffraction (XRD), using a Rigaku SmartLab diffractometer equipped with a one-dimensional high-speed Si strip detector (D/teX Ultra) and utilizing Cu *K*α radiation (40 kV and 30 mA). Structural refinements were

carried out by the Rietveld method with an iterative procedure using the software package PDXL-2 (Rigaku).

2.2 Electrochemical Measurements

The charge–discharge tests were performed with a Bio-Logic VSP potentiostat or a charge–discharge unit (HJ1001SD8, Hokuto Denko Corp.) using 2032-type coin cells assembled in an Ar-filled glove box. The working electrode was prepared by mixing $Na_2FeP_2O_7$, acetylene black (AB) as a conductive additive, and polytetrafluoroethylene (PTFE) as a binder in a weight ratio of 75:20:5. Metallic sodium discs (Aldrich, purity 99.95%) were pressed onto aluminum current collectors and used as reference and counter electrodes. A glass microfiber separator (Whatman GF/A) was impregnated under vacuum with the electrolyte at 363 K for one day prior to the test. Electrochemical impedance spectroscopy (EIS) measurements were carried out over a frequency range from 500 kHz to 1 mHz with a perturbation amplitude of 10 mV. Spectra were recorded upon assembling after a rest period of 12 h. For in situ XRD experiments, an air-tight cell with a Kapton window was used in combination with a temperature controller (Rigaku). The diffraction patterns were recorded at 363 K under vacuum. The electrochemical measurements were controlled with an ECAD-1000 charge–discharge system (EC Frontier Inc.).

3. Results and discussion

Owing to the high dissociative character of FSA^-, a homogeneous liquid state is achievable for the Na[FSA]–[C_2C_1im][FSA] system at room temperature over a wide compositional range (up to 50 mol% Na[FSA]) [20]. For comparison, the Na[TFSA]–[C_2C_1im][TFSA] (TFSA: bis(trifluoromethanesulfonyl)amide) system becomes saturated below a Na[TFSA] content of 30 mol% [10], underscoring the role of the anion in determining the liquidus concentration range. Although the ionic conductivity of the Na[FSA]–[C_2C_1im][FSA] IL (σ(IL)) decreases with increasing Na salt content, as shown in Table 1, a reasonably high value of 16.9 mS cm^{-1} is obtained at the highest concentration (50 mol% Na[FSA]) at 363 K. A drop in the bulk conductivity is broadly observed with increasing Na or Li salt concentrations in ILs, which is related to the increased viscosity [10,11,19,20,42]. These findings suggest that the addition of the Na salt leads to intensified ionic interactions and therefore hinders the liquid dynamics. The apparent transport number of Na^+ ($t'(Na^+)$) increases monotonously with the increase of Na[FSA], rising from 0.13 for 10 mol% to 0.35 for 50 mol% at 363 K. The values are slightly higher than those for the Na[FSA]–[C_3C_1pyrr][FSA]

system measured under similar conditions [19]. The Na^+ ion conductivity, $\sigma(Na^+)$, is an indicator of Na^+ ion transport in the IL and is calculated by multiplying σ(IL) and $t'(Na^+)$. The $\sigma(Na^+)$ values reach a maximum at 30 mol% Na[FSA], suggesting that the viscosity increases as electrolyte becomes more concentrated in Na^+ have a stronger impact on the resultant Na^+ transport properties than the increases $t'(Na^+)$.

To characterize the liquid structure at each concentration, Raman spectra were obtained for the Na[FSA]–[C_2C_1im][FSA] ILs at 298 and 363 K and assigned according to previous reports [10,43–46]. Clear spectral variations associated with the change of the anion environment were found in the frequency range of 680–800 cm^{-1}, as shown in Fig. 1 (see Fig. S1 for the entire spectrum in the range of 200–1600 cm^{-1}, Supplementary material). In this region, the Raman spectrum of the neat [C_2C_1im][FSA] shows a strong peak assigned to S–O stretching ($\nu_s(SO_2)$) at 726 cm^{-1}, which is derived from free uncoordinated FSA^- anions [43,44]. Upon the addition of Na[FSA], new bands appear at the higher frequency of 743 cm^{-1} at 298 K. With the increase of Na salt concentration, these newly appearing bands are gradually intensified at the expense of bands ascribable to the free FSA^-. Similar spectral variations were observed for the Li[FSA]–[C_2C_1im][FSA] ILs, in which the shift was slightly

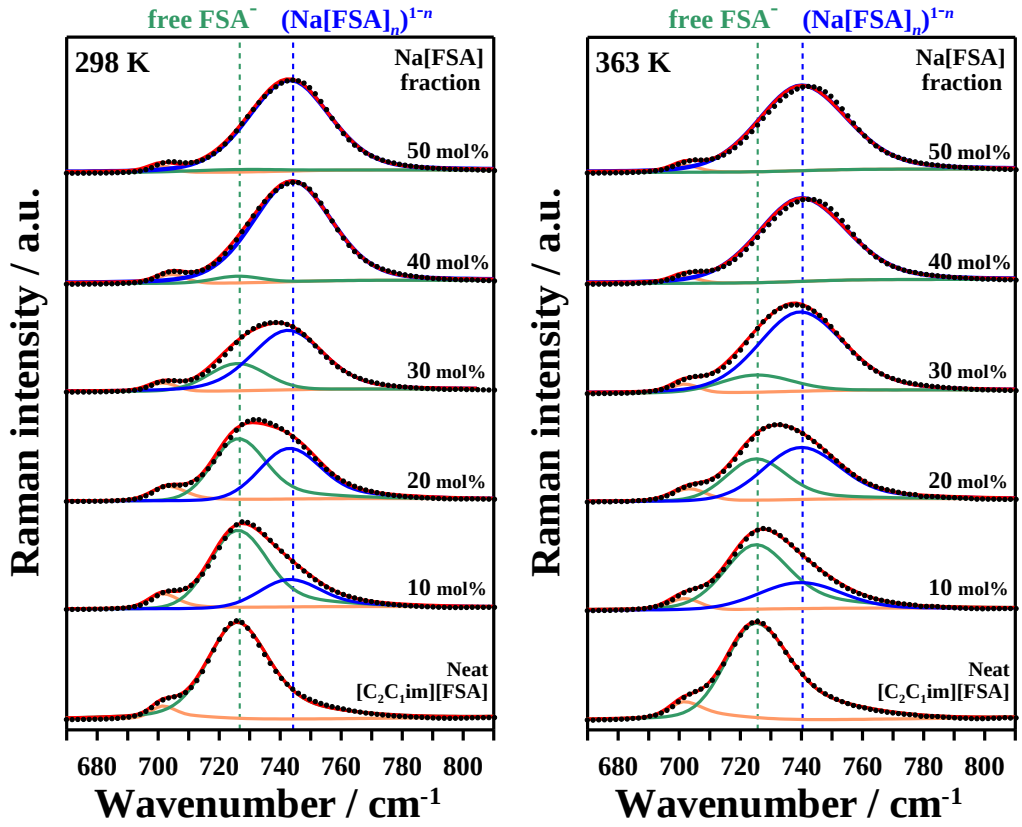

Fig. 1. Raman spectra of the Na[FSA]–[C_2C_1im][FSA] ionic liquids at Na[FSA] fractions of 0, 10, 20, 30, 40, and 50 mol% measured at 298 and 363 K. The dotted and red lines show the experimental and fitted spectra, respectively. The deconvoluted components of free FSA^-, bound FSA $(Na[FSA]_n)^{1-n}$, and $C_2C_1im^+$ are shown in green, blue, and orange, respectively.

larger than the values in the present case [43]. This is in agreement with the fact that the interaction is practically weaker in the Na[FSA]–[C_2C_1im][FSA] ILs owing to the larger size of Na^+ and reduced charge-to-size ratio as compared to Li^+ [10,45]. It is therefore plausible to assume that the new bands are associated with the coordination of FSA^- to Na^+, namely, the formation of $(Na[FSA]_n)^{1-n}$ charge-carrying complexes. It can be seen that the bound FSA^- amount surpasses the free FSA^- when the Na[FSA] fraction is increased from 20 to 30

mol%. Further increasing the Na salt to 40 and 50 mol% results in similar Raman spectra, in which only the bands of $(Na[FSA]_n)^{1-n}$ and $C_2C_1im^+$ are discernible, indicating that all the FSA^- is practically coordinated to Na^+. Fig. 1 also shows that the peak frequency for $(Na[FSA]_n)^{1-n}$ at 363 K (740 cm^{-1}) is lower than that observed at 298 K (743 cm^{-1}), suggesting that the coordination interaction between Na^+ and FSA^- is attenuated by rising temperature. It is noteworthy that Fujii et al. reported that one weakly solvated monodentate FSA^- of $(Li[FSA]_3)^{2-}$ could be liberated at 364 K. This finding is in stark contrast to the TFSA analogues in which the solvation number is independent of temperature [43]. For the Na[TFSA]–$[C_2C_1im][TFSA]$ ILs, the stable solvation structure was reported to be $(Na[TFSA]_3)^{2-}$ in the dilute Na concentration fraction range (10–30 mol%) [10]. Since the average number of FSA^- available to each Na^+ is less than 3 for the concentrated electrolytes (40 and 50 mol% Na), the Na^+ solvation structure should exist in an equilibrium between $(Na[FSA]_3)^{2-}$ and $(Na[FSA]_2)^-$. Forsyth and co-workers have also suggested that, for an IL with a high Na[FSA] fraction, there is a rapid exchange of the coordination environments of Na^+ which subsequently leads to a transport mechanism that arises from structural rearrangement of the system rather than vehicular diffusion of Na^+ in the dilute case [47]. In light of these

observations, either increasing the Na salt fraction or elevating the temperature over a certain threshold promotes the formation of a smaller Na^+ coordination sheath (e.g., $(Na[FSA]_2)^-$). The interfacial chemistry on the electrode surface therefore could be altered as a direct consequence of different Na^+ sheath structures. Because the desolvation (decomplexation) energetics is known to govern the Na^+/Li^+ ion transfer behavior at the electrolyte/electrode interface [48], the weak interaction between Na^+ and FSA^- at such a condition is supposed to facilitate the insertion reaction of Na^+ and the resulting battery performance. The structural changes may also affect the diffusion of Na^+ in the electrode mixture.

Fig. S2 shows the X-ray diffraction patterns of the $Na_2FeP_2O_7$ samples prepared under different conditions (either Ar or Ar/H_2 (95:5) atmosphere; with or without water washing). The Rietveld refinement results and the unit cell parameters determined for these samples are presented in Fig. S3–S6. The $Na_2FeP_2O_7$ prepared under Ar/H_2 (95:5) atmosphere contains $Na_4P_2O_7$ as an impurity (ca. 4.7%, according to the Rietveld analysis), whereas the sample prepared under Ar atmosphere was obtained in pure form. $Na_4P_2O_7$ is considered a thermodynamically stable phase in Na–Fe–P–O systems and has also been observed as an impurity in previous studies [34,38]. As a

straightforward method to remove the $Na_4P_2O_7$ impurity, the as-prepared samples were stirred in deionized water several times. After the water-washing treatment, phase-pure $Na_2FeP_2O_7$ was obtained without any visible traces of $Na_4P_2O_7$, as confirmed by the refined XRD patterns.

Fig. 2 shows the charge–discharge curves of the $Na_2FeP_2O_7$ samples synthesized under an Ar atmosphere measured in Na[FSA]–[C_2C_1im][FSA] IL at 363 K. The reversible capacity of 93 mAh g^{-1} is consistent with that acquired using the Na[FSA]–[C_3C_1pyrr][FSA] IL under the same conditions (vide infra). The stepwise voltage-capacity profiles observed are attributed to the presence of several distinct crystallographic Na sites within the $Na_2FeP_2O_7$ structure and

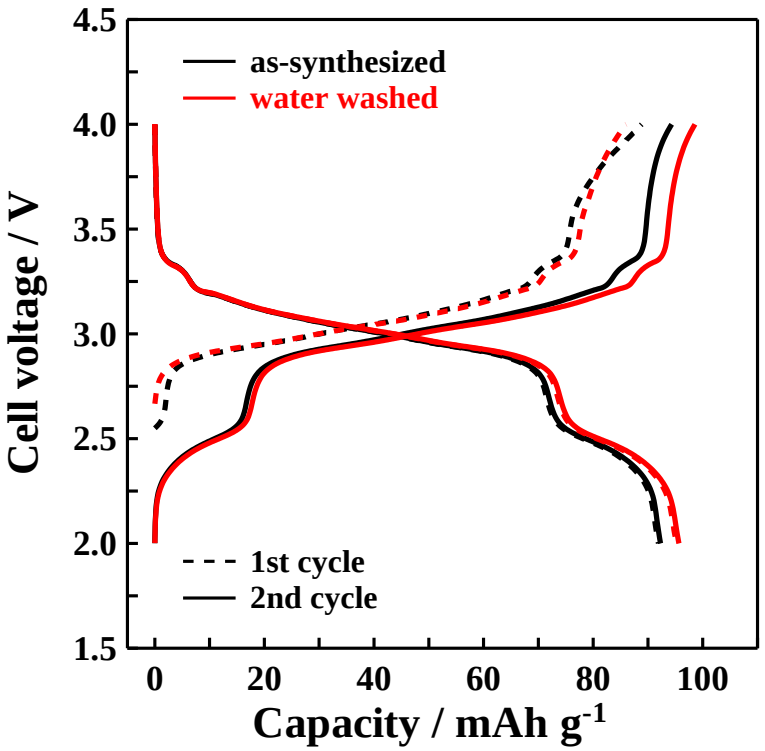

Fig. 2. Galvanostatic charge–discharge curves for the Na/Na[FSA]–[C_2C_1im][FSA]/$Na_2FeP_2O_7$ cell with 30 mol% Na[FSA] at 363 K. The

$Na_2FeP_2O_7$ sample used was synthesized under an Ar atmosphere followed by water washing. Each sample is shown as black and red lines, respectively. Cut-off voltage: 2.0–4.0 V. Current density: 10 mA g^{-1}.

their ordering [36]. Furthermore, a distinct drop (~0.08 V) between the first and subsequent charging profiles is observed, in agreement with previous studies [24,37,38]. Owing to the effective elimination of impurities by water washing, the reversible capacity increases from 93 to 96.5 mAh g^{-1}, closely approaching the theoretical capacity of 97 mAh g^{-1}.

The effects of the synthetic and electrode processing atmosphere on the Na stoichiometry of $Na_2FeP_2O_7$ was further investigated using charge–discharge tests, starting with discharging (pre-discharge), as proposed by Kim et al [37]. Spontaneous desodiation from $Na_2FeP_2O_7$ upon synthesis and/or processing was found, most likely caused by oxidative contamination on the particle surface with the formation of Fe^{3+}-containing phases (see Supplementary material for details). A closer look at the charge–discharge curves starting with discharge reveals that the voltage drop between the first charging and subsequent profiles no longer occurs, implying that the profile shift observed in Fig. 2 is caused by a Na deficiency in $Na_2FeP_2O_7$ (Fig. S7). The following electrochemical tests were performed using $Na_2FeP_2O_7$ synthesized under Ar atmosphere and water-washed.

The rate capability of the $Na_2FeP_2O_7$ electrode in the Na[FSA]–[C_2C_1im][FSA] IL was first investigated as a function of operating temperature, as shown in Fig. 3a. The data for the Na[FSA]–[C_3C_1pyrr][FSA] IL is also shown for comparison (Fig. 3b). The cells were charged to 4.0 V at a constant current of 10 mA g^{-1} and subsequently discharged to 2.0 V at various current densities from 20 to 4000 mA g^{-1}. The capacity decreases with increasing discharging rate in both the ILs at 298 K, whereas the rate capability of $Na_2FeP_2O_7$ is notably improved at temperatures greater than 323 K. For instance, the discharge capacities at 2000 mA g^{-1} substantially increase from 17 mAh g^{-1} at 298 K to more than 83 mAh g^{-1} for the cells tested at 323–363 K in the case of Na[FSA]–[C_2C_1im][FSA]. The difference in electrochemical performance between Na[FSA]–[C_2C_1im][FSA] and Na[FSA]–[C_3C_1pyrr][FSA] becomes unequivocal during high-rate tests, as the $Na_2FeP_2O_7$ electrode exhibits a higher discharge capacity in the former. The cell with the Na[FSA]–[C_2C_1im][FSA] IL shows a subtle capacity decline (< 3%) at 4000 mA g^{-1} when measured at 363 K, versus 19% observed for the Na[FSA]–[C_3C_1pyrr][FSA] IL. As shown in the discharge curves (Fig. S8), the polarization is considerably smaller in the Na[FSA]–[C_2C_1im][FSA] IL, highlighting the influence of the IL cation. This observation also indicates that

the rate determining step is not the Na^+ diffusion in the $Na_2FeP_2O_7$ since the difference in the ILs highly affects the performance. A similar trend has been

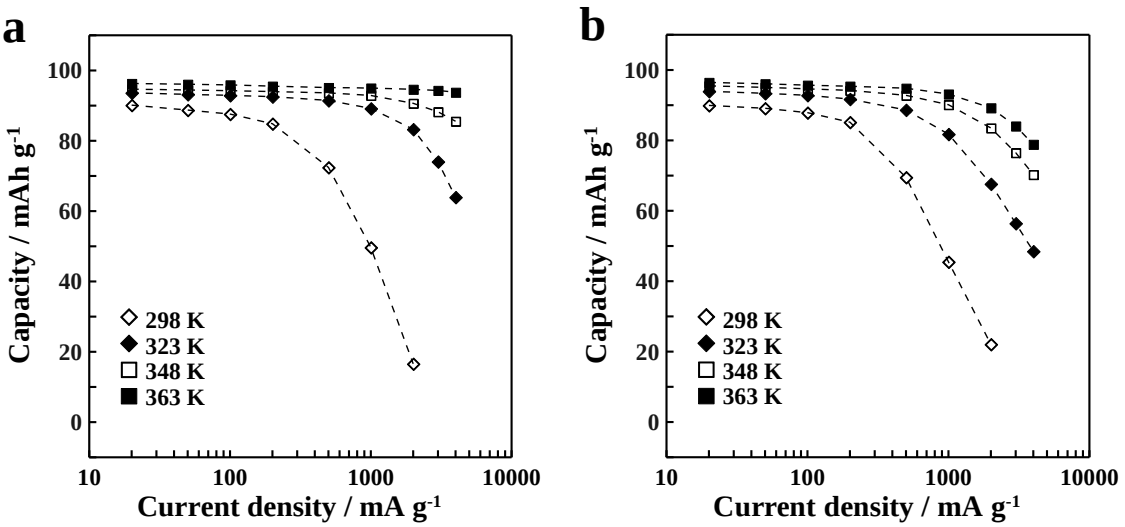

Fig. 3. Rate capabilities of the $Na_2FeP_2O_7$ positive electrodes over 298–363 K in the (a) Na[FSA]–[C_2C_1im][FSA] or (b) Na[FSA]–[C_3C_1pyrr][FSA] IL electrolytes with 30 mol% Na[FSA]. The $Na_2FeP_2O_7$ used was synthesized under an Ar atmosphere followed by water washing. The cell was charged at 10 mA g^{-1}. Cut-off voltage: 2.0–4.0 V.

reported for Li-ion batteries, in which the fast cycling of a $LiCoO_2$ cathode in Li-conducting [C_2C_1im][FSA] was realized, which could not be attained in the corresponding [C_3C_1pyrr][FSA] analogues [49]. Imidazolium-based IL electrolytes that generally exhibit a higher ionic conductivity than those of their pyrrolidinium or piperidinium analogues were thoroughly investigated for Li-ion battery applications. However, only a few examples using imidazolium-based IL electrolytes are available for Na secondary batteries [10,20]. This can be ascribed to the facts that the study of new electrolytes for

Na secondary batteries has received less attention and the current electrolyte choice is very limited [5].

To unravel the effect of the cationic structure on the cell, electrochemical impedance measurements were performed on $Na/Na_2FeP_2O_7$ half cells constructed with the Na[FSA]–[C_2C_1im][FSA] and Na[FSA]–[C_3C_1pyrr][FSA] IL electrolytes. Typical Nyquist plots for the imidazolium- and pyrrolidinium-based ILs are shown in Fig. 4. The high-frequency end of the plots relates to the ohmic portion of the impedance (R_b) and mainly includes the contribution from the ionic conductivity of the IL electrolytes. The mid-frequency region is generally associated with the charge-transfer process (R_{ct}) at the electrode/electrolyte interface [50]. The figure clearly shows that

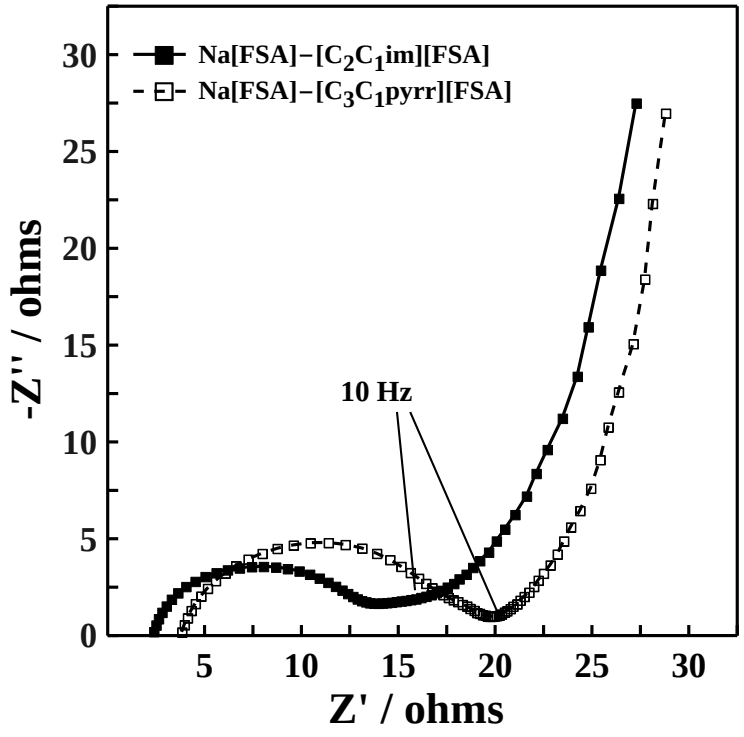

Fig. 4. Nyquist plots for the Na/Na[FSA]–[C_2C_1im][FSA]/$Na_2FeP_2O_7$ (solid symbols) and Na/Na[FSA]–[C_3C_1pyrr][FSA]/$Na_2FeP_2O_7$ (open symbols) cells at 363 K. The AC perturbation was 10 mV, and the frequency range was from 200 kHz to 100 mHz.

both the R_b and R_{ct} in the Na[FSA]–[C_2C_1im][FSA] IL are approximately two times lower than those observed in the Na[FSA]–[C_3C_1pyrr][FSA] IL, demonstrating that the former is beneficial toward efficient Na^+ transport in the electrolyte as well as electron transfer at the electrode interface, which together lead to the enhanced electrode kinetics.

Common approaches to improving the rate capabilities of cells include the nanostructuring and surface modification of the active materials and the reduction of electrode thickness; these strategies are generally used in tandem to maximize performance [51]. These methods have been adopted because the diffusion of Na^+ or Li^+ within the electrode has long been considered a sluggish process, and thus, the rate determining step [52,53]. On the other hand, various lines of evidence suggest that the electrolyte is the limiting factor for high rate performance [28,30,32,42,47]. MacFarlane and co-workers reported that the reaction kinetics of Li/$LiCoO_2$ cells in the Li[FSA]–[C_3C_1pyrr][FSA] IL showed better rate capability against that in a standard battery electrolyte (1.0 M $LiPF_6$ in EC:DMC), as the Li salt concentration of the electrolyte over a certain threshold (> 1.6 mol kg^{-1}) [42]. They ascribed the improved electrode

kinetics to the increase in Li^+ transference number with increasing Li-salt concentration. Yamada and co-workers revealed that a highly concentrated electrolyte (> 3.0 mol dm^{-3}) facilitated the ultrafast charging of Li/graphite cells. The rate capability far exceeded that in the currently used commercial electrolytes [30,32]. In the latter case, almost all solvent molecules and reaction-irrelevant ions were coordinated to Li^+, in contrast to a dilute electrolyte in which the majority of solvent molecules exist in a free state. The peculiar coordination sheath formed in concentrated electrolytes is postulated to facilitate Li^+ desolvation and charge transfer kinetics, realizing ultrafast intercalation.

Fig. 5 shows the charge–discharge results of the $Na_2FeP_2O_7$ electrode in the Na[FSA]–[C_2C_1im][FSA] IL with different Na salt fractions at 363 K. The polarization is considerably alleviated with the increase of Na[FSA] fraction, suggesting that the internal resistance (including bulk and/or interfacial impedance) decreases with increasing Na salt concentration, despite the high viscosity and low ionic conductivity of the concentrated systems. A pronounced difference is observed when the Na[FSA] content increases from 20 to 30 mol%. This may be related to a recent study in which Forsyth et al. revealed that the interfacial impedance of Na/Na symmetrical cells greatly decreased in

highly concentrated systems [47]. The cell with the most concentrated electrolyte (50 mol% Na[FSA]) exhibits a distinctly impressive rate capability,

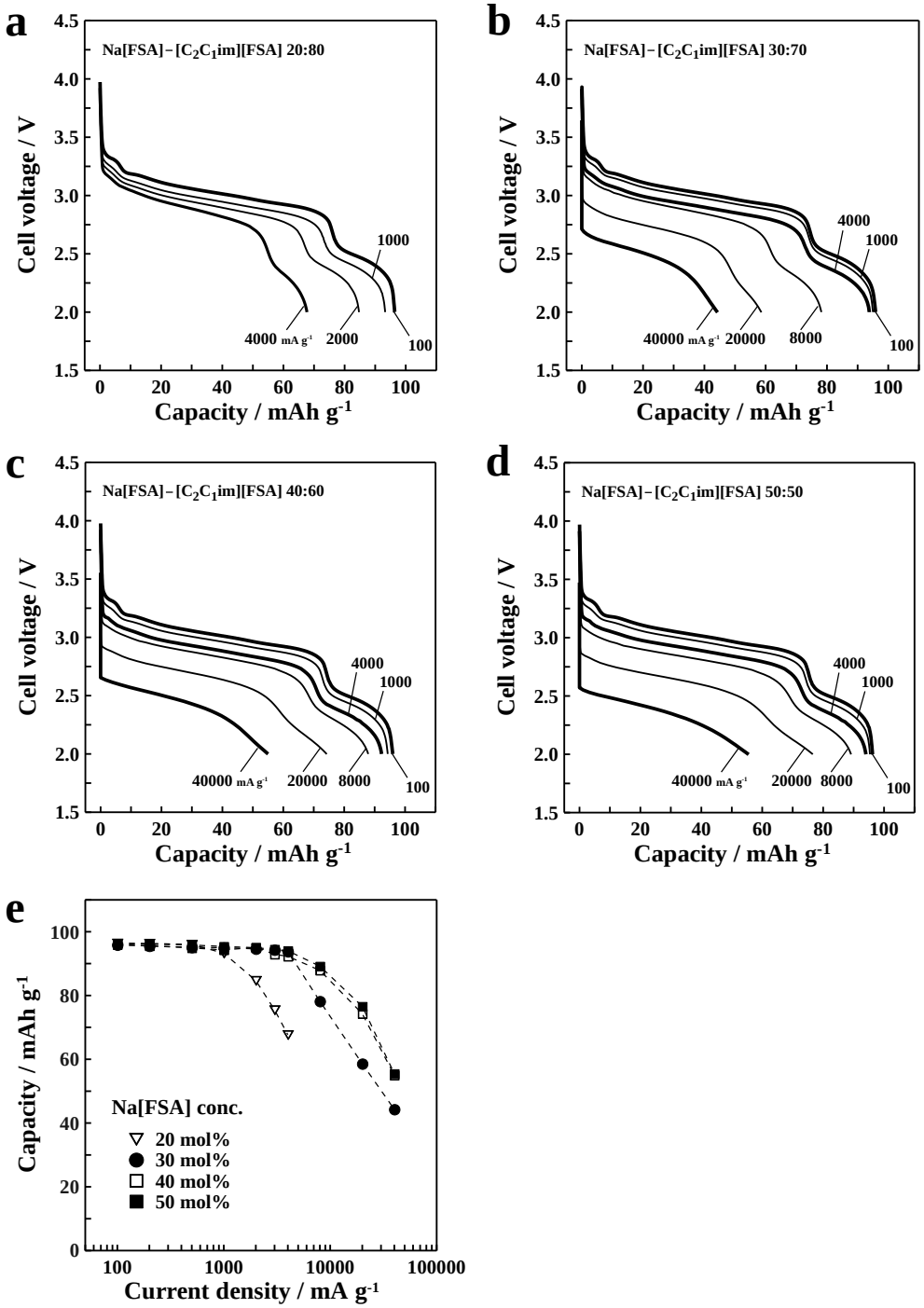

Fig. 5. Discharge curves for Na/Na[FSA]–$[C_2C_1im][FSA]$/$Na_2FeP_2O_7$ cells with different Na salt concentrations at various current densities ranging from 100 to 40000 mA g^{-1} at 363 K: (a) 20 mol%, (b) 30 mol%, (c) 40 mol%, and (d) 50 mol% Na[FSA]. (e) Rate capability of the $Na_2FeP_2O_7$ electrode in the Na[FSA]–$[C_2C_1im][FSA]$ IL as

a function of Na[FSA] concentration. The $Na_2FeP_2O_7$ sample used was synthesized under an Ar atmosphere followed by water washing. The cell was charged at 10 mA g^{-1}. Cut-off voltage: 2.0–4.0 V.

delivering capacities of 94, 89, 77, and 56 mAh g^{-1} at rates of 4000, 8000, 20000, and 40000 mA g^{-1}, respectively (Fig. 5d). This high rate capability far exceeds that of the 20 mol% cell (i.e., having the generally adopted concentration of ca. 1.0 M). As discussed above, $\sigma(Na^+)$ reaches the maximum at the Na[FSA] fraction of 30 mol%, suggesting that Na^+ transport in the bulk cannot account for this high rate capability in concentrated ILs. These findings imply that the aforementioned solution structures of the electrolytes, especially the $(Na[FSA]_n)^{1-n}$ charge-carrying complexes, play a dominant role in determining the resultant electrochemical behavior. This is supported by the nearly identical rate capabilities observed for the Na[FSA] fractions of 40 and 50 mol%, wherein similar FSA^- coordination modes were observed according to Raman spectroscopy. Furthermore, the rate determining step in the present study is therefore assumed to involve the interfacial decomplexation process of $(Na[FSA]_n)^{1-n}$, in contrast to the common belief that Na diffusion within the bulk electrolyte or electrode restricts the reaction kinetics. The preparation method for composite electrodes may also affect the Na^+ diffusion, and the study on this point is now underway.

An in situ XRD study was performed to investigate the structural changes of $Na_2FeP_2O_7$ during electrochemical cycling at 363 K; the results are shown in Fig. 6. The intense peak appearing at 38.3° and the diffuse background signal around 15–20° originate from the Al current collector and PTFE binder,

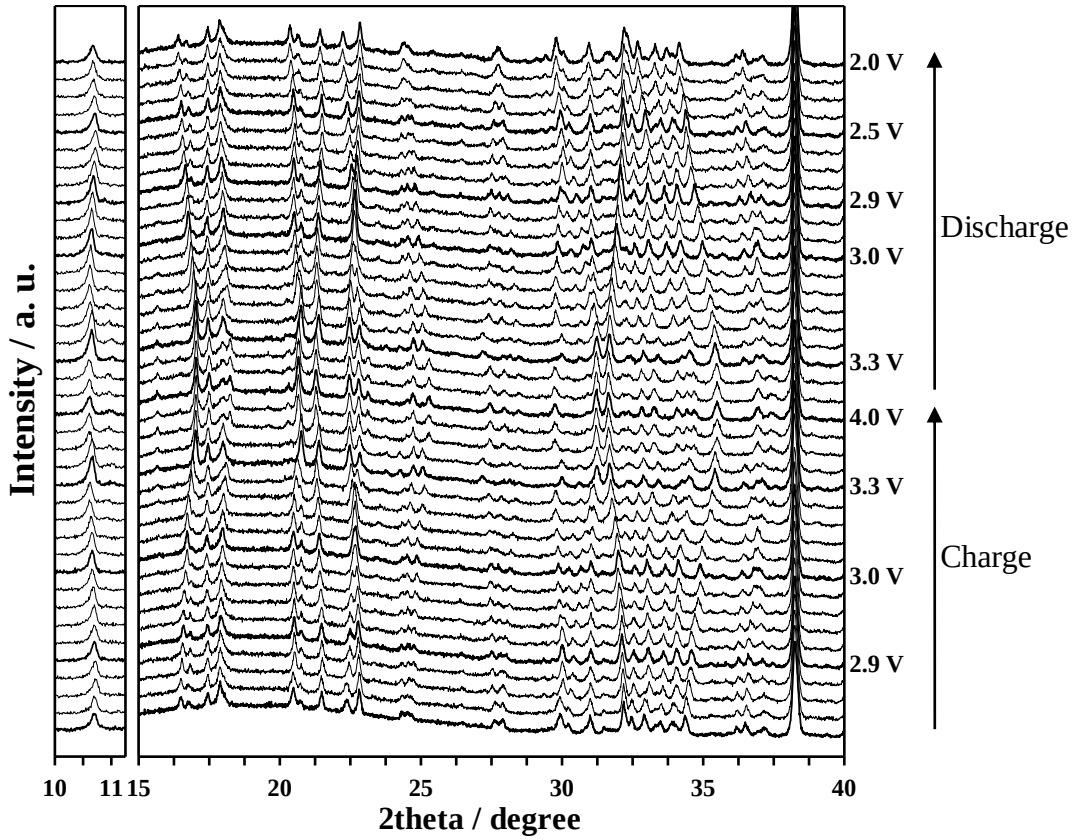

Fig. 6. In situ X-ray diffraction patterns of the $Na_2FeP_2O_7$ positive electrode recorded during the second charge–discharge cycle at 363 K. The intense peak at 38.3° originates from the Al current collector. Cut-off voltage: 2.0–4.0 V; current density: 5 mA g^{-1}.

respectively. The observed peak shifting is indicative of solid-solution behavior, although it does not vary continuously as a function of the amount of inserted Na ions. Concurrently, peak merging and splitting occur gradually when

charging to 4.0 V. Nevertheless, the change and shift of the Bragg peak positions appear to be completely reversible. Over the series of diffraction patterns for this $Na_2FeP_2O_7$ at 363 K, the appearance of a new phase at the expense of the other was not confirmed. Accordingly, Na insertion/extraction within the $Na_2FeP_2O_7$ proceeds without strong modification of the crystal framework, implying the possibility of a single-phase reaction [36]. Our XRD patterns are in good agreement with previously simulated results for which the most stable desodiated structures with different Na contents were optimized by density functional theory (DFT) calculations [37].

As shown in Fig. 7a, the combination of the structurally robust $Na_2FeP_2O_7$

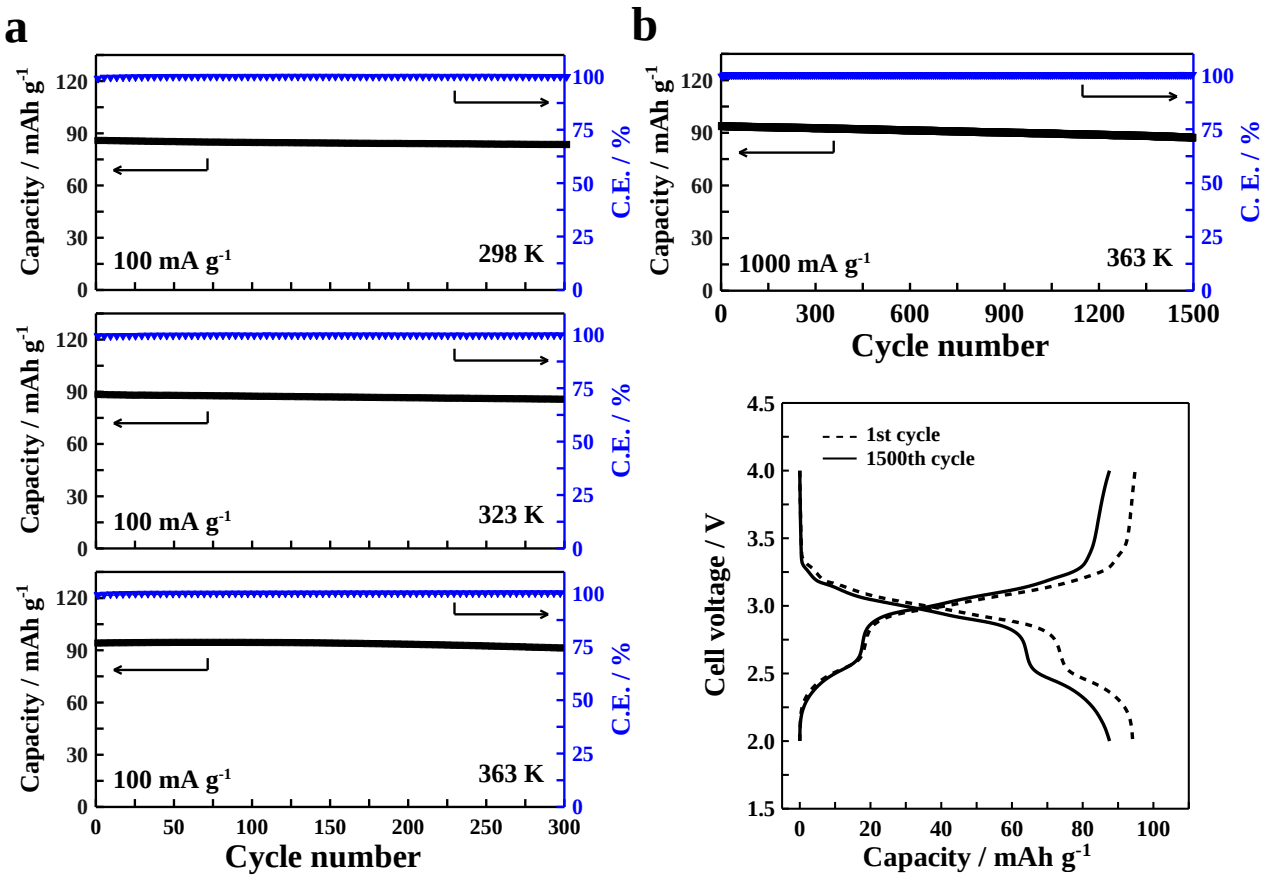

Fig. 7. Long-term electrochemical performance of the $Na_2FeP_2O_7$ positive electrode in the Na[FSA]–[C_2C_1im][FSA] IL electrolyte with 30 mol% Na[FSA]. (a) Cycle performance measured at 100 mA g^{-1} and 298–363 K. (b) Cycle performance measured at 1000 mA g^{-1} at 363 K. The charge–discharge curves at the 1st and the 1500th cycles are shown at the bottom. The $Na_2FeP_2O_7$ used was synthesized under an Ar atmosphere followed by water washing. Cut-off voltage: 2.0–4.0 V.

electrode and the Na[FSA]–[C_2C_1im][FSA] electrolyte leads to fairly stable cyclability at a moderate rate of 100 mA g^{-1} over 298–363 K, as evidenced by the satisfactory capacity retention (> 97% after 300 cycles) and averaged coulombic efficiency (>99.5%). Al corrosion has been a long-standing issue facing the battery community in designing new electrolytes, especially for the selection of Na/Li salts [5,33]. Although the detailed mechanism is unclear, it is

generally accepted that the solubility of passivation products ($(Al[FSA]_x)^{3-x}$ or $(Al[TFSA]_x)^{3-x}$ complexes) in a given electrolyte dominate the progression of Al corrosion [29,33]. Since ILs are composed entirely of ions that possess low dissolution ability, Al corrosion is effectively inhibited, as was demonstrated by a recent experiment comparing the corrosion behavior of an Al substrate in Na[FSA]–propylene carbonate and Na[FSA]–[C_3C_1pyrr][FSA] [54]. As shown in Fig. 7b, the cell also exhibits great potential for continuous high-rate operation at 363 K. Nearly the full capacity can be well sustained within a rate of 1000 mA g^{-1}, which corresponds to a charge/discharge time of less than 6 min. Even at this extreme condition, the capacity retention and averaged coulombic efficiency after 1500 cycles are as high as 93% and 99.9%, respectively.

4. Conclusions

In summary, we found that Na secondary batteries with ultrahigh rate capability and long life can be achieved by using highly concentrated FSA^--based IL electrolytes and a $Na_2FeP_2O_7$ positive electrode with three-dimensional Na^+ diffusion paths. Raman spectral analysis revealed that a synergistic effect of the concentration and temperature on the Na^+ coordination sheath structure resulted in altered interfacial

chemistry and electrochemical characteristics in comparison to the dilute system. The cell can operate at a current density that is higher than most known Na secondary batteries [11–13] applying an IL electrolyte by two or three orders of magnitude (e.g., 20000 mA g^{-1}). Fairly stable cyclability up to 1500 cycles with nearly 100% coulombic efficiency at 1000 mA g^{-1} was also demonstrated. This work conclusively reveals that increasing Na salt fraction in the IL electrolyte and elevating the working temperature over a certain threshold can be an easy-to-use strategy for Na secondary batteries, simultaneously satisfying safety- and performance-related requirements.

Acknowledgements

This study was partly performed under a management of the Advanced Low Carbon Technology Research and Development Program (ALCA) of the Japan Science and Technology Agency (JST) and "Elements Strategy Initiative for Catalysts & Batteries (ESICB)" supported by the Japanese Ministry of Education, Culture, Sports, Science and Technology (MEXT) program "Elements Strategy Initiative to Form Core Rersearch Center" (since 2012).

References

[1] D. Larcher, J. M. Tarascon, Nat. Chem. 7 (2015) 19–29.
[2] M. S. Islam, C. A. J. Fisher, Chem. Soc. Rev. 43 (2014) 185–204.
[3] M. D. Slater, D. Kim, E. Lee, C. S. Johnson, Adv. Funct. Mater. 23 (2013)

947–958.
[4] N. Yabuuchi, K. Kubota, M. Dahbi, S. Komaba, Chem. Rev. 114 (2014) 11636–11682.
[5] A. Ponrouch, D. Monti, A. Boschin, B. Steen, P. Johansson, M. R. Palacin, J. Mater. Chem. A 3 (2015) 22–42.
[6] A. Ponrouch, R. Dedryvere, D. Monti, A. E. Demet, J. M. A. Mba, L. Croguennec, C. Masquelier, P. Johansson, M. R. Palacin, Energy Environ. Sci. 6 (2013) 2361–2369.
[7] S. M. Oh, S. T. Myung, C. S. Yoon, J. Lu, J. Hassoun, B. Scrosati, K. Amine, Y. K. Sun, Nano Lett. 14 (2014) 1620–1626.
[8] M. Armand, F. Endres, D.R. MacFarlane, H. Ohno, B. Scrosati, Nature Mater. 8 (2009) 621–629.
[9] D. R. MacFarlane, N. Tachikawa, M. Forsyth, J. M. Pringle, P. C. Howlett, G. D. Elliott, J. H. Davis, M. Watanabe, P. Simon, C. A. Angell, Energy Environ. Sci. 7 (2014) 232–250.
[10] D. Monti, E. Jonsson, M.R. Palacin, P. Johansson, J. Power Sources 245 (2014) 630–636.
[11] H. Yoon, H. J. Zhu, A. Hervault, M. Armand, D. R. MacFarlane, M. Forsyth, Phys. Chem. Chem. Phys. 16 (2014) 12350–12355.
[12] I. Hasa, S. Passerini, J. Hassoun, J. Power Sources 303 (2016) 203–207.
[13] N. Wongttharom, C. H. Wang, Y. C. Wang, C. H. Yang, J. K. Chang, ACS Appl. Mater. Interfaces 6 (2014) 17564–17570.
[14] Y. H. Xu, Y. J. Zhu, Y. H. Liu, C. S. Wang, Adv. Energy Mater. 3 (2013) 128–133.
[15] Y. J. Zhu, Y. H. Xu, Y. H. Liu, C. Luo, C. S. Wang, Nanoscale 5 (2013) 780–787.
[16] A. Fukunaga, T. Nohira, Y. Kozawa, R. Hagiwara, S. Sakai, K. Nitta, S. Inazawa, J. Power Sources 209 (2012) 52–56.
[17] C. S. Ding, T. Nohira, K. Kuroda, R. Hagiwara, A. Fukunaga, S. Sakai, K. Nitta, S. Inazawa, J. Power Sources 238 (2013) 296–300.
[18] C. S. Ding, T. Nohira, R. Hagiwara, K. Matsumoto, Y. Okamoto, A. Fukunaga, S. Sakai, K. Nitta, S. Inazawa, J. Power Sources 269 (2014) 124–128.
[19] K. Matsumoto, Y. Okamoto, T. Nohira, R. Hagiwara, J. Phys. Chem. C 119 (2015) 7648–7655.
[20] K. Matsumoto, T. Hosokawa, T. Nohira, R. Hagiwara, A. Fukunaga, K. Numata, E. Itani, S. Sakai, K. Nitta, S. Inazawa, J. Power Sources 265 (2014) 36–39.
[21] C. Y. Chen, K. Matsumoto, T. Nohira, R. Hagiwara, Electrochem. Commun. 45 (2014) 63–66.
[22] C. Y. Chen, K. Matsumoto, T. Nohira, R. Hagiwara, J. Electrochem. Soc. 162

(2015) A2093–A2098.
[23] C. Y. Chen, K. Matsumoto, T. Nohira, R. Hagiwara, J. Electrochem. Soc. 162 (2015) A176–A180.
[24] C. Y. Chen, K. Matsumoto, T. Nohira, C.S. Ding, T. Yamamoto, R. Hagiwara, Electrochim. Acta 133 (2014) 583–588.
[25] A. Fukunaga, T. Nohira, R. Hagiwara, K. Numata, E. Itani, S. Sakai, K. Nitta, J. Appl. Electrochem. 46 (2016) 487–496.
[26] S. K. Jeong, M. Inaba, Y. Iriyama, T. Abe, Z. Ogumi, J. Power Sources 175 (2008) 540–546.
[27] L. M. Suo, Y. S. Hu, H. Li, M. Armand, L. Q. Chen, Nat. Commun. 4 (2013) 1481.
[28] J. F. Qian, W. A. Henderson, W. Xu, P. Bhattacharya, M. Engelhard, O. Borodin, J. G. Zhang, Nat. Commun. 6 (2015) 6362.
[29] D. W. McOwen, D. M. Seo, O. Borodin, J. Vatamanu, P. D. Boyle, W. A. Henderson, Energy Environ. Sci. 7 (2014) 416–426.
[30] Y. Yamada, K. Furukawa, K. Sodeyama, K. Kikuchi, M. Yaegashi, Y. Teteyama, A. Yamada, J. Am. Chem. Soc. 136 (2014) 5039–5046.
[31] R. Petibon, C. P. Aiken, L. Ma, D. Xiong, J. R. Dahn, Electrochim. Acta, 154 (2015) 287–293.
[32] Y. Yamada, M. Yaegashi, T. Abe, A. Yamada, Chem. Commun. 49 (2013) 11194–11196.
[33] Y. Yamada, A. Yamada, J. Electrochem. Soc. 162 (2015) A2406–A2423.
[34] P. Barpanda, T. Ye, S. Nishimura, S.C. Chung, Y. Yamada, M. Okubo, H. S. Zhou, A. Yamada, Electrochem. Commun. 24 (2012) 116–119.
[35] J. M. Clark, P. Barpanda, A. Yamada, M. S. Islam, J. Mater. Chem. A 2 (2014) 11807–11812.
[36] P. Barpanda, G. Liu, C.D. Ling, M. Tamaru, M. Avdeev, S.C. Chung, Y. Yamada, A. Yamada, Chem. Mater. 25 (2013) 3480–3487.
[37] H. Kim, R.A. Shakoor, C. Park, S.Y. Lim, J.S. Kim, W. Cho, K. Miyasaka, R. Kahraman, Y. Jung and J. W. Choi, Adv. Funct. Mater. 23 (2013) 1147–1155.
[38] T. Honma, A. Sato, N. Ito, T. Togashi, K. Shinozaki, T. Komatsu, J. Non-Cryst. Solids 404 (2014) 26–31.
[39] C. Y. Chen, K. Matsumoto, T. Nohira, R. Hagiwara, Y. Orikasa, Y. Uchimoto, J. Power Sources 246 (2014) 783–787.
[40] J. Evans, C. A. Vincent, P. G. Bruce, Polymer 28 (1987) 2324–2328.
[41] K. M. Abraham, Z. Jiang, B. Carroll, Chem. Mater. 9 (1997) 1978–1988.
[42] H. Yoon, P. C. Howlett, A. S. Best, M. Forsyth, D. R. MacFarlane, J. Electrochem. Soc. 160 (2013) A1629–A1637.

[43] K. Fujii, H. Hamano, H. Doi, X. D. Song, S. Tsuzuki, K. Hayamizu, S. Seki, Y. Kameda, K. Dokko, M. Watanabe, Y. Umebayashi, J. Phys. Chem. C 117 (2013) 19314–19324.

[44] K. Fujii, S. Seki, S. Fukuda, R. Kanzaki, T. Takamuku, Y. Umebasyashi, S. Ishiguro, J. Phys. Chem. B 111 (2007) 12829–12833.

[45] G. A. Griffin, A. Moretti, S. Jeong, S. Passerini, J. Phys. Chem. C 118 (2014) 9966–9973.

[46] H. Yoon, A. S. Best, M. Morsyth, D. R. MacFarlane, P. C. Howlett, Phys. Chem. Chem. Phys. 17 (2015) 4656–.

[47] M. Forsyth, H. Yoon, F. Chen, H. Zhu, D. R. MacFarlane, M. Armand, P. C. Howlett, J. Phys. Chem. C 120 (2016) 4276–4286.

[48] M. Okoshi, Y. Yamada, A. Yamada, H. Nakai, J. Electrochem. Soc. 160 (2013) A2160–A2165.

[49] H. Matsumoto, H. Sakaebe, K. Tatsumi, M. Kikuta, E. Ishiko, M. Kono, J. Power Sources 160 (2006) 1308–1313.

[50] A. Funabiki, M. Inaba, Z. Ogumi, S. Yuasa, J. Otsuji, A. Tasaka, J. Electrochem. Soc. 145 (1998) 172–178.

[51] J. J. Wang, X. L. Sun, Energy Environ. Sci. 5 (2012) 5163–5185.

[52] K. T. Lee, J. C. Lytle, N. S. Ergang, S. M. Oh, A. Stein, Adv. Funct. Mater. 15 (2005) 547–556.

[53] Y. Tang, Y. Zhang, W. Li, B. Ma, X. Chen, Chem. Soc. Rev. 44 (2015) 5926–5940.

[54] L. Otaegui, E. Goikolea, F. Aguesse, M. Armand, T. Rojo, G. Singh, J. Power Sources 297 (2015) 168–173.